ADVANCED MATERIALS TECHNOLOGIES
www.advmattechnol.de

Flexible Bioelectronic Devices Based on Micropatterned Monolithic Carbon Fiber Mats

Maria Vomero, Calogero Gueli, Elena Zucchini, Luciano Fadiga, Johannes B. Erhardt, Swati Sharma, and Thomas Stieglitz**

Polymer-derived carbon can serve as an electrode material in multimodal neural stimulation, recording, and neurotransmitter sensing platforms. The primary challenge in its applicability in implantable, flexible neural devices is its characteristic mechanical hardness that renders it difficult to fabricate the entire device using only carbon. A microfabrication technique is introduced for patterning flexible, cloth-like, polymer-derived carbon fiber (CF) mats embedded in polyimide (PI), via selective reactive ion etching. This scalable, monolithic manufacturing method eliminates any joints or metal interconnects and creates electrocorticography electrode arrays based on a single CF mat. The batch-fabricated CF/PI composite structures, with critical dimension of 12.5 µm, are tested for their mechanical, electrical, and electrochemical stability, as well as to chemicals that mimic acute postsurgery inflammatory reactions. Their recording performance is validated in rat models. Reported CF patterning process can benefit various carbon microdevices that are expected to feature flexibility, material stability, and biocompatibility.

1. Introduction

Neurological disorders have placed an economic burden on western ageing societies.[1] Bioelectronics medicine[2] and neurotechnologies[3] promise alternative treatment options to pharmaceutical therapies. Microsystems engineering acts as emerging technology in neural implants to establish interfaces to the nervous system[4,5] with high spatial resolution and small footprints. The material–tissue interaction is critical for the success of these implants.[6,7] In the recent years, electrocorticography (ECoG) electrodes have been established as compromise between invasiveness and spatial selectivity. When they are flexible and able to conform to curvilinear bodies, they allow for high amplitude recordings up to the resolution of spikes[8–11] even if the Young's modulus of the device is orders of magnitude higher than the tissue underneath.[12] Surface biocompatibility of the implant materials ensure intended interactions with the target cells.[5,13–15]

In the recent past, carbon has gained considerable attention as a neural electrode material owing to its inertness and biocompatibility, ability to serve as multimodal platform for recording, stimulation, and neurotransmitter detection.[16,17] Various sp^2-rich carbon materials are cytocompatible,[18–20] corrosion resistant, electrically conductive, and electrochemically stable.[21,22] Carbon-based ECoG electrodes have been successfully tested as multimodal electrode material[23,24] utilizing graphene flakes,[25] carbon nanotubes (CNTs),[18] glassy carbon,[16,26] and carbon fibers (CFs).[27] Recently there has been a lot of progress in the field of graphene-based transparent flexible devices.[28] Graphene and CNTs generally entail

Dr. M. Vomero, C. Gueli, J. B. Erhardt, Prof. T. Stieglitz
Laboratory for Biomedical Microtechnology
Department of Microsystems Engineering-IMTEK
University of Freiburg
Freiburg 79110, Germany
E-mail: Thomas.stieglitz@imtek.uni-freiburg.de
Dr. M. Vomero, Prof. T. Stieglitz
BrainLinks-BrainTools Center
University of Freiburg
Freiburg 79110, Germany
The ORCID identification number(s) for the author(s) of this article can be found under https://doi.org/10.1002/admt.201900713.

DOI: 10.1002/admt.201900713

E. Zucchini, Prof. L. Fadiga
Center for Translational Neurophysiology of Speech and Communication
Istituto Italiano di Tecnologia (IIT)
Via Fossato di Mortara 17/19, 44121 Ferrara, Italy
E. Zucchini, Prof. L. Fadiga
Section of Human Physiology University of Ferrara
Via Fossato di Mortara 17/19, 44121 Ferrara, Italy
Dr. S. Sharma
Institute of Microstructure Technology
Karlsruhe Institute of Technology
Hermann-von-Helmholtz-Platz 1, 76344
Eggenstein-Leopoldshafen, Germany
E-mail: swati@iitmandi.ac.in
Dr. S. Sharma
School of Engineering
Indian Institute of Technology Mandi
Kamand, Mandi 175005, Himachal Pradesh, India
Prof. T. Stieglitz
Bernstein Center Freiburg
University of Freiburg
Freiburg 79110, Germany

cumbersome fabrication processes[25] and pose potential cytotoxicity concerns.[29] Moreover, carbon nanomaterials available in the powder forms are often patterned employing additive manufacturing techniques such as printing,[28] which require additional compatibility analysis of the binder or glue that is used for preparing the inks. Glassy carbon is the endorsed choice since it is composed of strongly interconnected graphene-like structures rather than discrete nanounits[30] and allows for simple photolithographic patterning.[22] Additionally, it exhibits magnetic resonance (MR)-compatibility[20] due to its relatively low electrical conductivity and low magnetic susceptibility.[31] The use of glassy carbon in neural devices is currently limited to electrode sites due to its lack of flexibility. Other device components still rely on thin metal films, leading to a compromised interface durability[32,33] and work-function differences.[34] Few studies report on laser-induced carbonization of different polymers in order to achieve flexible structures.[35,36] This serial process shows large variation in material composition depending on process and material parameters.[35] Consequently, such methods are currently unsuitable for reliable large-scale manufacturing of implantable neural probes.

Pyrolyzed electrospun polyacrylonitrile (PAN) fibers are widely used in electrochemical devices.[37,38] They are well-known for their mechanical strength[39] and cytocompatibility.[40] The challenge, however, is to micropattern the cloth-like fiber mats. To our knowledge, there is no report on direct microstructuring of CF mats after carbonization. Structuring the precarbonized (PAN) fibers has been attempted by modifying the electrospinning set-up[41] and by changing the polymer viscosity.[42] Such methods are usually limited in tolerances and resolution and are not suitable for neural implant manufacturing.

Here we report on a micropatterning technique based on reactive ion etching (RIE) of CFs embedded in polyimide. Entire ECoG electrode arrays were seamlessly manufactured from a single CF mat. In this wafer-scale process, we achieved CF structure resolution down to 12.5 μm in-plane and ≈3 μm in height. These ultraflexible neural devices showed mechanical and electrochemical stability as well as MR compatibility in vitro, and exhibited excellent recording performance in vivo.

2. Results and Discussions

CF microelectrode arrays featuring different diameters were patterned employing an extensively optimized sequence of widespread micromachining techniques on 4 in. wafers with a high precision and the ability to scale electrode and array size. Prefabricated CF mats, prepared by electrospinning of PAN followed by pyrolysis at 940 °C (temperature profile shown in Figure S1a, Supporting Information) were sandwiched between two layers of PI that eventually serve as both, substrate and insulation layers.

Electrospinning is one of the most common techniques for the large-scale, low cost fabrication of the CFs that accounts for ≈80% of the commercial CF production.[43] The microstructure and properties of such fibers have been extensively investigated and it has been reported that they feature an excellent mechanical strength,[39] electrochemical stability,[44] and chemical inertness.[45] Unfortunately, this stability also renders it difficult to pattern polymer-derived CFs employing common microfabrication techniques. Consequently, in microdevices such as neural sensors, CFs are often only used as bundles or ropes sliced through their cross-section.[27,46] Patterning microscale features on CF mats allows for a complete utilization of their surface area as well as flexibility, without the need for any additional material for fabricating the contact pads. In other words, one can obtain an entire device—and not just electrodes—by micropatterning the CF mats. To achieve this, one can also pattern the polymer fiber mats prior to their carbonization. In this regard, lithographic patterning of electrospun SU-8 fiber mats has been reported.[47] However, due to its poor viscoelasticity, SU-8 only yields relatively short fibers that do not intertwine well or convert into large cloth-like sheets. One also needs to factor in the pyrolytic shrinkage that can lead to altered shapes or undesirable adhesion on to silicon substrate making it difficult to detach the structures. PAN fibers, on the other hand, are several millimeters long and yield mechanically strong CF mats on pyrolysis. The method reported here offers yet another advantage of integrating PI into the CF mats before micropatterning. It is essential for neural probes that the PI is uniformly distributed through the fibers, without any trapped bubbles.

Polymer-derived carbon is hard to machine due to its brittleness, but there are reports on its micropatterning using FIB milling, RIE, laser milling and electrochemical etching.[22] These methods, however, have only been utilized to pattern glassy carbon films, which is significantly different from fibers. For example, glassy carbon film etching is often only carried out for surface patterning (i.e., only a few micrometers of carbon are removed from the top of a thick film), while in the case of CF mats, the material is etched all the way through the bottom PI substrate. The presence of solidified PI between the fibers prevents them from moving due to tensile pulling during the etch, thus making it possible to pattern precise shapes.

In order to obtain the desired geometries, CF mats were embedded and patterned using a combination of photolithography, lift-off and etching (**Figure 1**). First, a base PI layer was spin-coated onto a silicon wafer and was soft-cured at 120 °C. A second PI layer was coated onto this and used uncured as a substrate for placing the prefabricated CF mat of 3 μm thickness (Figure 1a–c). The base PI layer provided the mechanical support during fabrication, while the uncured PI on the top allowed for a bubble-free integration of the CFs mat due to a low viscosity and ease of filling in the voids between the fibers through capillary action. After curing the entire assembly at 450 °C (temperature profile shown in Figure S2b, Supporting Information), an aluminum mask of reversed geometry was patterned via resist lift-off (Figure 1d–f). This CF/PI composite was then micropatterned using oxygen plasma RIE (Figure 1g) for 60 min. The etch rate for PI (200 nm min^{-1} at 100 W) was found to be approximately four times higher than that of the CFs. Hence, the etch duration was calculated according to CF etch rate. Once the CFs were etched away, no traces of PI were observed on the substrate. Notably, in order to carry out RIE for 60 min, a robust metal mask is essential for selective etching of CFs. It is also preferred to have a mask that can be washed away in aqueous solutions (e.g., caustic etch bath in the case of aluminum), such that mask removal does not affect the PI. In the subsequent steps, shown in Figure 1h–j, the CF micropatterns were insulated with PI on top and device outline, fenestrations

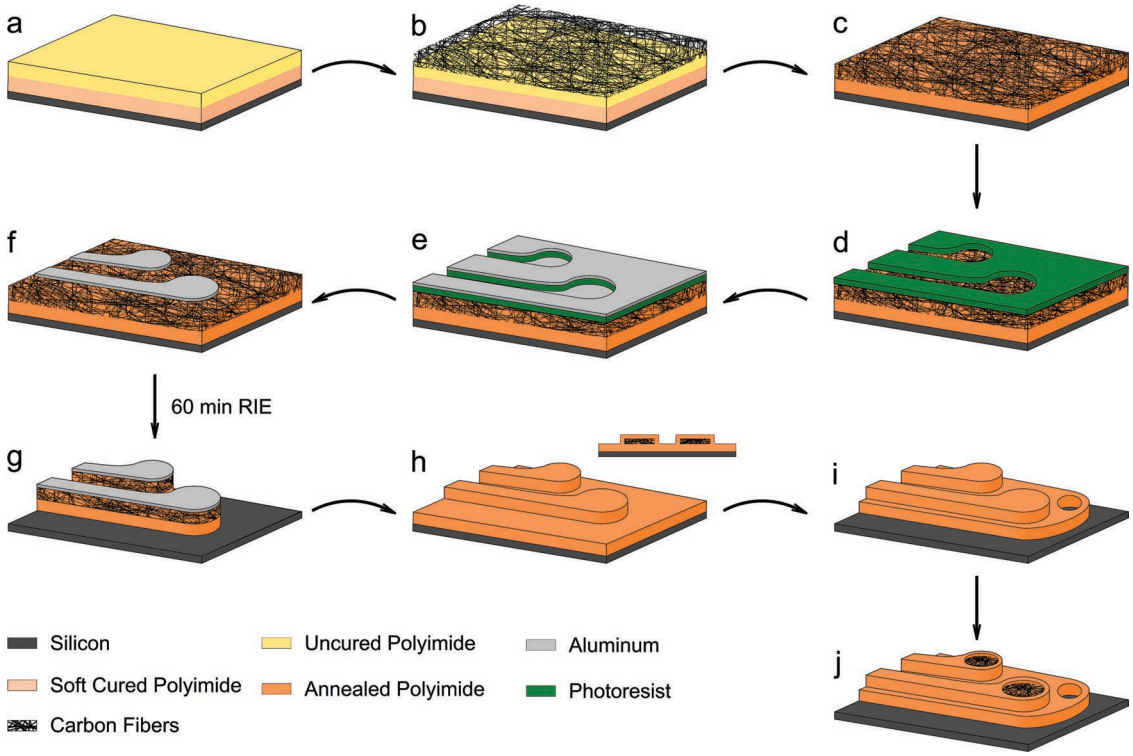

Figure 1. Fabrication protocol for CF/PI neural probe. a–c) Embedding CF mat into soft-cured/uncured PI, followed by curing, d–f) patterning aluminum mask (positive design) onto CF/PI surface via resist lift-off, g) structures after RIE, h) aluminum mask removal and insulation with PI (see inset for cross-section). Creation of i) device outline and fenestrations, and j) recording site openings by lithographic masking followed by RIE of PI and resist removal (individual steps not shown).

and recording site openings were created using lithography and RIE. Resulting joint-free carbon arrays were individually peeled-off from the silicon carrier for further use and characterization of their mechanical and electrochemical properties.

Prior to final designs, multiple test patterns at different process stages were characterized and their yield was optimized. PAN fibers were oxidized and converted into CFs via pyrolysis employing well-established protocols that yield a disordered turbostratic carbon material after undergoing nitrogen-assisted cyclization (**Figure 2**a–c). Compatibility of CF mats with differently annealed PI (uncured, partially cured, and fully cured) was also evaluated and it was found that the CF-PI interface was most uniform and robust in the case of uncured PI, likely due to its low viscosity (SEM images shown in Figure 2d,e). Raman spectrum of the CFs (Figure 2f) indicated the presence of two major first order Raman bands, *D* and *G*, at 1360 and 1580 cm^{-1}, respectively (intensity ratio, I_D/I_G: ≈1), along with a broad second order 2D overtone around 2700 cm^{-1}. The *D*-band (A_{1g} breathing mode of the hexagonal rings activated by defects) reveals the presence of a disordered component, while the *G*-band (E_{2g} mode at the Γ-point resulting from stretching of C—C bond) suggests a primarily sp^2 hybridization in the material.[48] This is in line with the Raman characteristics of most nongraphitizing polymer-derived carbons.[49] The presence of sp^2 characteristics along with disordered regions indicates that the carbon features a short-range order with a predominantly turbostratic structure. The electrical and electrochemical properties of such carbons are suitable for the purpose of neural stimulation recording.

After confirming the microstructure, a CF mat was placed between two PI sheets and scanning transmission electron microscope (STEM) images of the cross-sectional profile were acquired (Figure 2g,h). Evidently, the CFs were oriented in all directions and there were no air bubbles trapped between them.

The implantable probes fabricated by the aforementioned process offer versatile applications in the field of bioelectronics medicine. For example, in addition to neural activity recording, such platforms can be utilized for simultaneous electrical stimulation and monitoring of dopamine levels (**Figure 3**a). These devices enable the use of two remarkably attractive properties of pyrolytic carbon, its wide electrochemical stability window and chemical inertness, which make it superior to metals in various biomedical applications.

Flexible arrays (Figures 2c and 3b) featuring recording sites of four different diameters (30, 50, 100, and 200 μm) were characterized for their morphology using optical profilometry (Figure 3d). Electrical connection and assembly to electrical equipment was performed in this pilot study using a zero-insertion force (ZIF) connector mounted on a printed circuit board (PCB). The array showed flexibility and adhered on the tapered surface of a pipette tip (Figure 3e,f). As it can be observed, it is highly flexible and all four electrode-containing fingers could be independently bent at different angles.

One of the most desirable features in neural interface is their compliance to the mechanical properties of the host tissue. It is important that ECoG arrays conform to brain without the need of applying external forces,[12,50] which is influenced by the flexibility as well as the footprint of the implanted structures. It has

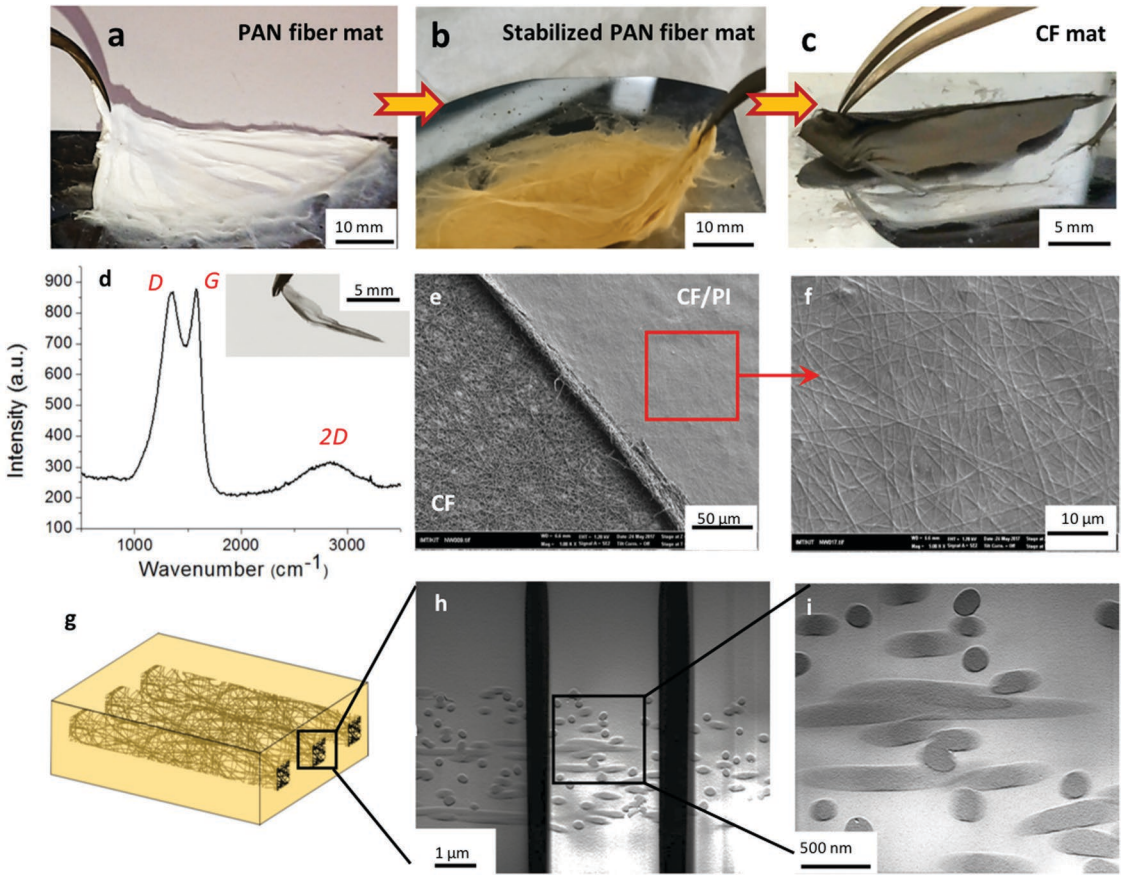

Figure 2. Fabrication and characterization CF mats. a–c) Optical images of PAN fiber mats after (a) electrospinning, (b) oxidative stabilization, and (c) carbonization. d) Raman spectrum of carbon fiber mat. e,f) Scanning electron images of test patterns showing a CF mat embedded in PI. g–i) Cross-sectional images of the carbon fiber patterns showing (g) a schematic, and (h,i) scanning transmission electron microscope (STEM) images of the device cross-section.

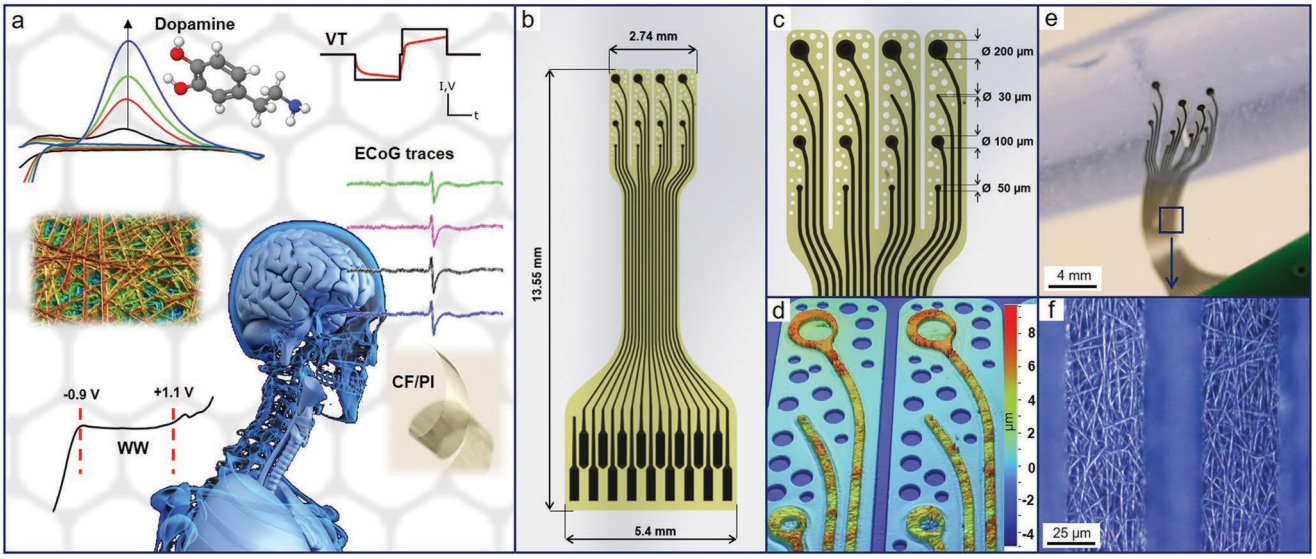

Figure 3. Applications and characterization of CF-based flexible device. a) A schematic showing the multimodal approach (recording, stimulation, electrochemical neurotransmitter detection) of flexible carbon devices carbon in potential bioelectronics medicine applications, b) sketch of the entire CF/PI neural probe, c) sketch of the electrode array, d) optical profilometry image of part of the electrode array with opened electrodes and fenestrations, e) neural electrode inserted into a zero insertion force connector (ZIF) on a printed circuit board (PCB) and pressed against the tapered surface of a pipette tip, and f) optical microscopy of patterned CF interconnects.

been shown that, despite a much-reduced invasion compared to penetrating electrodes, ECoG devices do experience foreign-body response and glial scar formation which ultimately leads to the encapsulation and subsequent loss of functionality of the implants. The mechanically dissimilar implant components (i.e., flexible substrate and stiff electrode sites) also tend to delaminate over time.[33] A fiber-based morphology of the conductive tracks and electrode sites dramatically lowers risk of crack formation and propagation due to its much-enhanced flexibility (see Figure S2 and Video S1, Supporting Information). The individual fingers are designed fenestrated—and thus "breathable"—to allow for the diffusion of biological fluids through the device and conformability and improve the tissue–electrode contact. Moreover, even if some of the fibers unexpectedly break and get disconnected, other fibers remain percolated and the overall device maintains a reasonable electron transport. Cloth-like electrode structures can be freely bent and twisted in all directions, and adjust their geometry to conform to the tissue.

In order to evaluate the mechanical robustness of our PI substrate, test structures were manufactured to resemble its design (without CFs; mentioned as "patterned" geometry) and were characterized via pull test to understand the durability of the PI/PI interface under different designs and curing conditions. For this purpose, first, the base layer was fully cured (FC) before a second PI layer was spin-coated and patterned onto it (see illustrations in **Figure 4**a). Another similar structure was prepared where the base PI was only partially cured (250 °C, see Figure S1b, Supporting Information) before coating the second layer, and the two layers were cured together (designated PC in Figure 4a). Given the particular shape (striped) of the bottom PI layer in our protocol, it seemed important to understand if the patterned design could influence the mechanical properties of the PI substrate when compared to an unpatterned design, and if the one-step curing of the two layers could be beneficial for the devices. For this experiment, samples made of two unpatterned PI sheets were used as controls.

After implantation, medical devices are also inevitably exposed to the highly humid and oxidative physiological environment. The most critical time frame is the first week of implantation, during which the acute tissue inflammatory reaction takes place and reactive oxygen species are secreted with the aim of attacking and eventually destroying the foreign device.[51,52] It is therefore important to verify the ability of an implantable device to keep its integrity and mechanical stability after undergoing aging treatments mimicking physiological concentration of H_2O_2.[53] For this purpose, the mechanical tests performed on the test structures were repeated on similar but aged structures, kept in 30×10^{-3} M H_2O_2 for 7 days at 37 °C. Pyrolytic CFs feature an excellent thermal stability and thermal shock resistance,[22] and can therefore withstand a variety of high or low temperature sterilization methods (e.g., steam sterilization in an autoclave and ethylene oxide treatment).

Results indicated that pristine (as fabricated) samples have higher stress at fracture than the aged ones, independent of their design and curing protocol (for details see Figure 4a and Table S1, Supporting Information). The average stress at fracture of the patterned samples is higher than the average stress calculated for the control or unpatterned samples, both when the two PI layers are curing together and separately (PC and FC protocols, respectively). Indeed, the one-step curing appears to be beneficial for the patterned design, and thus for the final flexible carbon devices. The pull test performed here to evaluate the reliability of design chosen for our thin-film fully flexible carbon electrodes substantiated the fact that it requires no compromise on the mechanical payoff of the devices.

To assess the flexibility and strength of the CF/PI composite, tensile bending tests were performed on test structures composed of a CF mat on PI substrate. For this purpose, the CF mat was placed on a PI layer before curing, and this composite was thermally treated at 450 °C and cut into 0.5×1 cm^2 rectangular pieces (Figure 4b; Table S2, Supporting Information). The top PI layer was intentionally not incorporated so as to ensure that the CF mat was directly exposed to the aging solution. Prior to starting the bending test, the CF/PI samples were optically investigated for ensuring the integrity of the fibers and a good initial interlock with the PI. The electrical resistance of the pristine (as fabricated) CF/PI test structures was measured after 10, 50, and 100 k bending cycles with a radius of curvature of 3 mm (Figure 4b). Also in this case, the same measurements were repeated on aged samples, using the aforementioned protocol, which were evaluated for any change in their electrical resistance over bending cycles.

Evidently, the increase in resistance due to the bending of the CFs was negligible for both pristine and aged samples. However, from the beginning, the aged samples exhibited slightly higher resistance than the pristine ones. Their optical characterization (Figure 4c–e) confirmed the presence of occasional structural deformation in the CF mat (i.e., the fiber network was disrupted). Considering that the average resistance of the aged samples did not significantly vary throughout the bending test, it is reasonable to assume that minor structural damages may have been caused by handling of the samples during repeated rinsing and drying procedure following the aging bath, rather than the chemical effect of H_2O_2 on the fibers. Any significant chemical modification would lead to a constant increase in the electrical resistance over the bending cycles, which was not observed in our experiments.

A CF/PI sample, similar to the ones used for the tensile bending tests, was subjected to a 3T magnetic resonance imaging (MRI) scan and compared to clinical ECoG strip electrodes, flexible laser structured metals with a thickness of about 25 µm embedded in polydimethyl siloxane and thin-film metal-based polyimide probes (300 nm platinum). Image artefacts of our carbon-based samples were negligible, despite the amount of CF was larger than in the other samples (see Figure S3, Supporting Information). Therefore, CF/PI probes can be combined with high-field MR imaging, based on the given results.

The manufactured 4×4 flexible carbon electrode arrays were designed such that each electrode row features a different diameter, ranging from 30 to 200 µm. After releasing the devices from the silicon wafer, they were inserted into a board-mounted ZIF connector and were electrochemically characterized. The CFs exposed at the contact pads were able to withstand the force exerted by the internal springs of the ZIF connector without breaking or being visibly damaged. Electrochemical impedance spectroscopy (EIS) and cyclic voltammetry (CV) were performed on all four electrode diameters in phosphate buffered saline (PBS) solution. The excitation voltage used for the EIS was 100 mV and the frequency ranged between 1 Hz

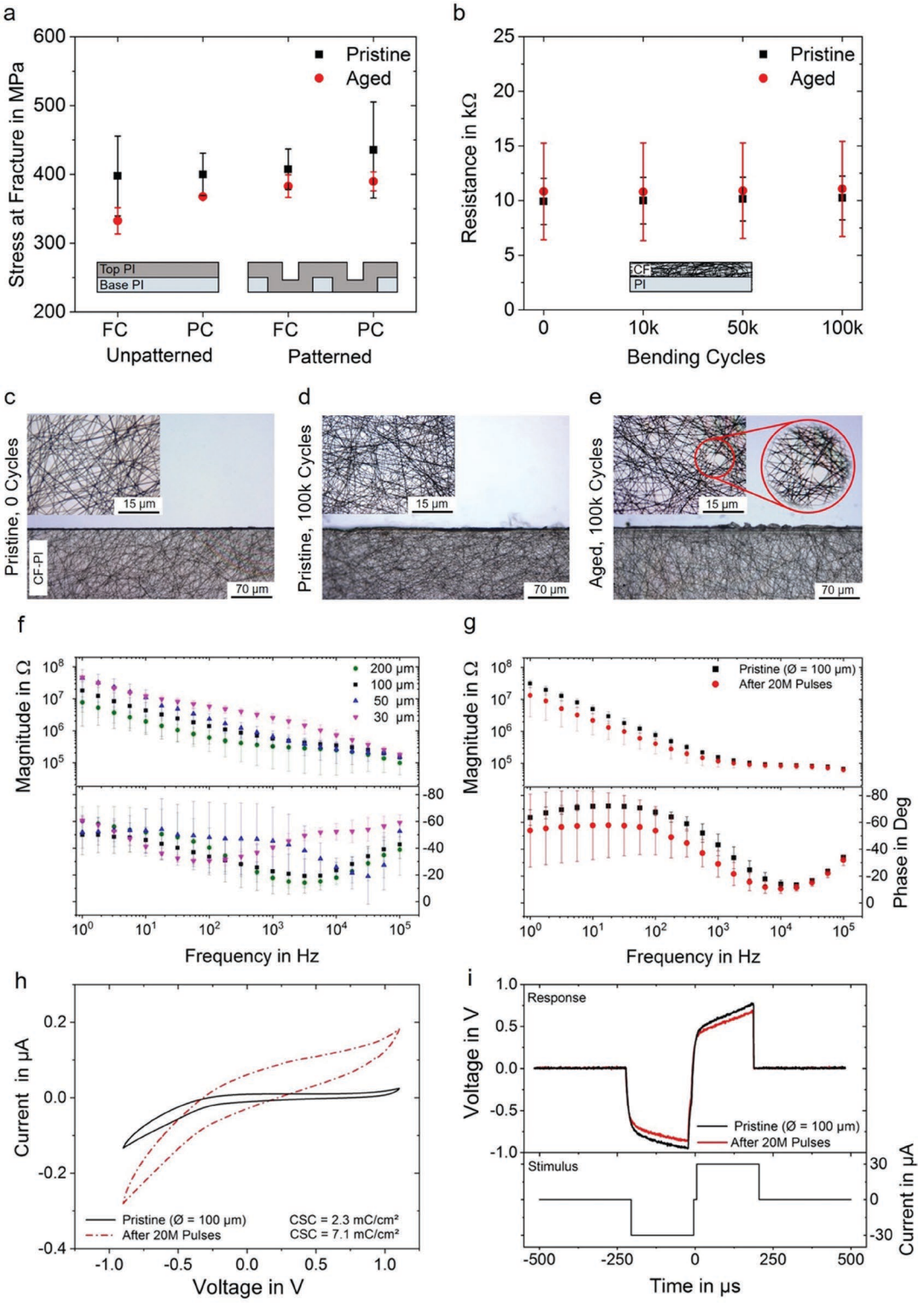

Figure 4. Mechanical characterization of PI/PI and CF/PI composites with and without aging. a) Stress at fracture of PI structures resembling the substrate design surrounding the carbon fibers (patterned) and unpatterned PI layers as control, b) electrical resistance of the CF/PI test structures, pristine, and aged in 30 mmol H_2O_2 for 7 days at 37 °C, after cyclic bending with a radius of 3 mm, c–e) optical microscopy images of the CF/PI test structures, pristine, aged, and after carrying out the bending experiments. Electrochemical characterization. f) Bode Plot obtained from the EIS measurements of four electrodes per diameter belonging to six different ECoG arrays, g) 100 µm diameter CF electrodes electrically stimulated with 20 million charge-balanced biphasic current pulses with charge density of 19 µC cm^{-2}, h) cyclic voltammogram ran within the CF electrodes water window (–0.9 to 1.1 V), before and after stimulation, i) voltage transient measured at the electrode/electrolyte interface before and after stimulation.

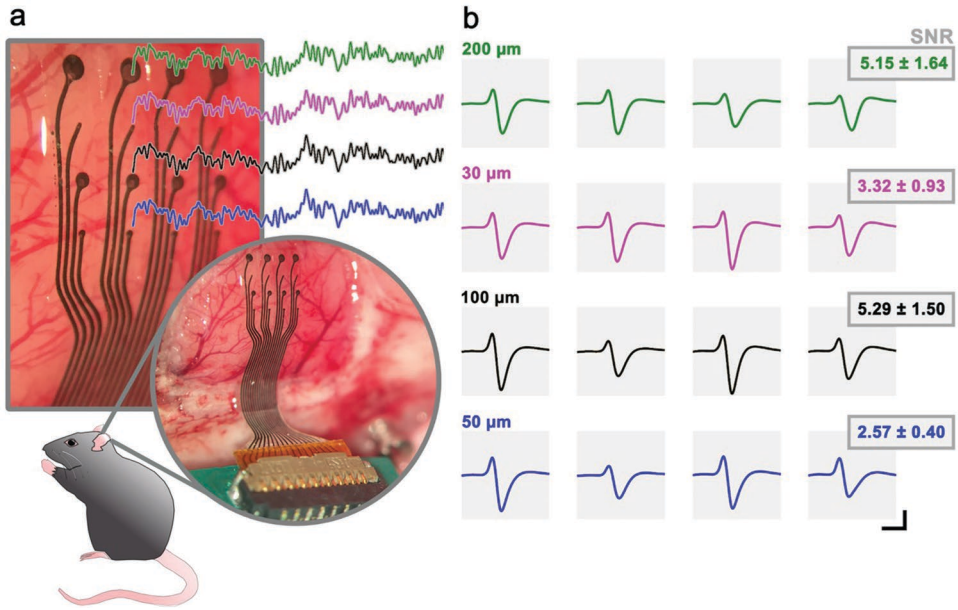

Figure 5. In vivo characterization of CF-based flexible neural implants. a) Digital photograph of the device implanted over the rat barrel cortex with representative band-pass filtered traces (3–300 Hz) detected by the different electrode diameters during spontaneous activity. b) Somatosensory evoked potentials map of one representative position (average of 60 trials, data filtered between 3 and 300 Hz, scale bar: 500 µV–20 ms). Reported signal-to-noise ratio of each electrode diameter corresponds to the mean ± standard error of mean of the three recorded positions.

and 100 kHz. Bode plots were obtained from the EIS measurements of four electrodes per diameter belonging to six different ECoG arrays (Figure 4f; Table S3, Supporting Information). As expected, the impedance magnitude is a function of the electrode diameter (the larger the electrode, the lower the impedance). Variability between electrodes of one diameter is higher for larger electrodes, most likely due to a higher variability of exposed fibers counting for the real surface area compared to the geometric surface area. The shape of both magnitude and phase corresponds to the Randles model.[54] At high frequencies (>1 kHz) the impedance is mainly determined by the resistive component, while at low frequencies (<1 kHz) it becomes more capacitive. Cyclic voltammograms of the electrodes are presented in Figure S5 of the Supporting Information. The 100 µm diameter CF electrodes were electrically stimulated with 20 million charge-balanced biphasic current pulses with charge density of 76.4 µC cm^{-2} in order to activate their surface and study their behavior under electrical load. Average impedance magnitude dropped after stimulation but maintained the same shape, while the phase showed a more pronounced constant phase characteristic at low frequencies (Figure 4g). This behavior is consistent with what has been previously observed in other studies on the activation of glassy carbon ECoG electrodes via electric pulses.[15,33,55] The charge storage capacity, determined from the area of the CV ran within the CF electrodes water window (–0.9 to 1.1 V, also see Figure S4, Supporting Information) increased from 2.3 to 7.1 mC cm^{-2} after stimulation (Figure 4h; Figure S5, Supporting Information), which is another known sign of activation.

Voltage transients were measured at the electrode/electrolyte interface during current-controlled stimulation. The amplitude of the voltage response did not significantly change after the 20 million pulses, remaining within the water window (Figure 4i). The maximum negative and positive voltage became less negative and less positive, respectively, assessing again a general improvement of the electrochemical performance of the CF electrodes after stimulation (and thus proving their activation).

After mechanical and electrochemical characterization, a fully flexible CF-based ECoG device was tested in a rat model. The device was implanted over the rat primary somatosensory barrel field (S1BF) in three different positions to test the ability of all the electrode areas to record neural activity. Both spontaneous brain activity (**Figure 5**a) and somatosensory evoked potentials (SEPs, Figure 5b) were recorded from all the electrodes. Signal-to-noise ratio (SNR) was calculated in order to investigate whether the CF electrodes can discriminate evoked activity from spontaneous brain signals. All the electrodes diameters were able to record high-quality SEPs with extremely big peak-to-peak amplitudes (in the mV range, Figure 5b). This was confirmed by the SNR values (data shown in Figure 5b) which resulted to be significantly high especially for the 200 and 100 µm diameter electrodes. In fact, the power of the evoked activity recorded by these electrodes was fivefold larger than the background noise (i.e., spontaneous brain activity). Smaller electrodes (50 and 30 µm), in accordance with their impedance, exhibited lower SNR values when compared to the large ones but were still able to clearly discriminate evoked activity from the spontaneous. Respective mean spectrograms showing the frequency content of the evoked neural signals are presented in Figure S6 of the Supporting Information.

3. Conclusions

We have demonstrated a simple and scalable batch fabrication technique for micropatterning CF mats monolithically

embedded in PI, which is currently tested down to a feature size of 12.5 µm. The metal-free, all polymer/carbon neural probes fabricated using this technique demonstrated excellent stability and in vivo biocompatibility along with a good recording performance. The focus of this work was ECoG electrodes, however, this technology can also be used for the fabrication of other types of implants, such as deep brain stimulation electrodes intracortical shaft electrodes, cuffs or transverse intrafascicular multichannel electrodes for peripheral and autonomous nerves. As the entire device is composed of the CF/PI composite, there are no interfaces with metals. This not only improves the device durability, but also lowers the risk of undesirable error such as that caused by poor electrical contact or work function differences. This work also confirms that the CF/PI interface is very stable, and can survive a large number of bending cycles and exposure to strong oxidants.

Reported fabrication process gives a whole new direction to carbon-based flexible device fabrication. In addition to neural probes, the technique can be used to fabricate a variety of flexible bioelectronic devices such as implantable biosensors, biofield-effect-transistors, bioelectronic nose, and biochemical monitoring systems. The applications can be further extended to in vitro cell culture and activity monitoring platforms, energy storage devices, and other wearable electronics. The characteristic high surface-to-volume ratio of the fibers has various proven advantages in the context of micro/nanodevices that entail an enhanced electrical and mechanical performance as well as sensitivity. The cloth-like structure of the CF mats provides a superior flexibility and conformability, even in the case of high curvatures. Reported process steps are simple, free of hazardous chemicals, involve reasonably low-cost equipment, and are easy to scale-up. While most polymeric carbon based microdevices are obtained by patterning the polymer prior to carbonization, a new concept of patterning carbon itself is presented in this work. It is expected that the extensive process optimization, structural stability tests, and the validation of in vivo device performance detailed in this contribution will immediately benefit microdevice research in many emerging and established scientific disciplines.

4. Experimental Section

Device fabrication and Characterization: Fiber Mat Preparation and Characterization: A 10 wt% solution of PAN (Sigma, Germany) was prepared in dimethylformamide and electrospun onto a silicon wafer, using a nylon cloth spacer between the wafer and the fiber mat, on a commercial electrospinner (IME Technologies EC-CLI Electrospinner, Netherlands) to achieve ≈20 µm thick PAN fiber mats. Average diameter of CFs was 328 ± 50 nm and the surface-to-volume ratio was 12.2×10^6 m^{-1}, as computed from optical image of a fiber mat using ImageJ software (see details in the Supporting Information). The fiber mats were released from the cloth and placed between two Al_2O_3 plates prior to being stabilized by oxidation at 220 °C for 120 min. Stabilized PAN fiber mats were then carbonized in a Carbolite CTF/65/55 tube furnace under nitrogen flow with a temperature ramp rate of 5 °C min^{-1} at 940 °C for 60 min, followed by natural cooling. Raman spectroscopy was performed on a Bruker Senterra confocal Raman microscope using DPSS excitation laser (λ = 532 nm) at 2 mW power at five different locations on the CF mat. SEM imaging was carried out on a Carl Zeiss AG-SUPRA 60VP SEM set-up. Sample preparation of CF/PI sandwich structures and STEM analysis were carried out on a focused ion beam/secondary electron microscope system FEI Dual Beam Strata 400S equipped with a STEM detector. A thin slice of the sample was milled using Ga ion beam and placed onto a transmission electron microscopy sample holder. Due to the similar scattering properties of CFs and PI, bright field-STEM images were recorded at low primary electron energy of 30 keV for a better contrast by enhancing electron scattering properties.

Device Manufacture: A 2 µm thick layer of PI (U-Varnish S, UBE) was spin-coated onto another silicon wafer and soft-cured at 120 °C for 3 min. A second layer of PI was then spin-coated onto the first one using the same protocol (9000 rpm for 30 s) and a CF mat was placed on it before performing another soft cure. The two-step PI layering guarantees that the CF mat anchors to the uncured (and thus highly viscous) PI without sinking too deep into the base PI layer. As a result, the CFs are well insulated at the bottom but still partially exposed at the top. The CF/PI composite was subsequently annealed at 450 °C for 15 min. The patterning of the CF/PI composite was done by oxygen plasma RIE. Etch mask was prepared by lift-off process (also see Figure 1). For metal deposition and subsequent lift-off, 4 µm of negative tone photoresist ma-N-1440 (micro resist technology GmbH, Germany) was spin-coated at 3000 rpm, exposed at 16.7 mW cm^{-2} on an MA6 mask aligner (Süss Microtec SE, Germany) and developed in ma-D-550-S (micro resist technology GmbH, Germany) for 240 s. 200 nm of Al was sputtered with an UNIVEX 500 (Leybold GmbH, Germany) sputtering machine at 200 W and lift-off of the photoresist was done in acetone to obtain a metal mask for patterning the CF/PI composite. Subsequently, RIE was carried out at a power of 100 W, a plasma frequency of 13.56 MHz, a pressure of 30 mTorr and a gas flow of 50 sccm in six runs of 10 min. To remove the metal mask, the wafers were placed in Al etching solution TechniEtch Al80 (MicroChemicals GmbH, Germany) for 30 s at 40 °C on a hot plate and then rinsed with deionized water.

For the top insulation, a 4 µm thick layer of PI was spin-coated at 4500 rpm on the patterned CF/PI structures and fully cured at 450 °C for 15 min. Prior to this, the base PI was activated by oxygen plasma at a power of 80 W, a plasma frequency of 13.56 MHz, a pressure of 80 mTorr and a gas flow of 50 sccm for 30 s (STPS Technologies, United Kingdom). For structuring the outlines of the devices, 24 µm of positive tone resist AZ9260 (MicroChemicals GmbH, Germany) was applied in two steps. Each step consisted of spin-coating one layer of photoresist at 1600 rpm for 30 s and curing it for 10 min at 100 °C on a hot plate. After UV-light exposure (9 mW cm^{-2}), the resist was developed in AZ400K (MicroChemicals GmbH, Germany) diluted 1:3 with deionized water, for 4.5 min. RIE was performed in a two-step process for 5 min at 200 W followed by 35 min at 100 W. The openings for active sites and connection pads were structured with only one layer of the AZ9260 photoresist and then etched with RIE for 2.5 min at 200 W followed by 14 min at 100 W. Outlines and openings were structured in two separate steps for precise tailoring of the active site openings and preventing to over-etch the fibers. The devices were finally mechanically released from the silicon wafer.

Device Characterization: Measurements with an optical profilometer (Wyko NT9100 Optical Profilometer, Veeco/Bruker) were performed to obtain information on the height and wall-coverage of the structures.

Mechanical Tests and Interface Durability: Pull Test: Samples were designed to resemble the geometry of the devices (patterned PI on unpatterned PI). The samples are H-shaped with the middle-part to be pulled (2.5 × 5 mm^2) and perpendicular parts (each 12 × 5 mm^2) to be held by the clamp mechanism of the pull tester. Consisting of two layers of U-Varnish S PI, two groups of samples were fabricated as given below.

Group FC: 1) Spin-coating of the base PI and full cure (450 °C, 15 min). 2) Patterning of the base with RIE through a lithographically structured photoresist mask (AZ9260). 3) The base PI was then activated by RIE for 30 s at 80 W for better adhesion of the subsequent layer. 4) Spin-coating of the top PI, 5) full cure, and 6) patterning following the same protocol used for the base layer. As a control, samples with the same outer shape and thickness are fabricated, consisting of two unpatterned PI layers (without the trace-resembling structure).

Group PC: Similar to Group FC with the exception that the base PI was not fully cured (step 5) but only partially cured at a temperature

of 250 °C (temperature that allows evaporation of solvents and further processing). This type of samples was used to evaluate the effect of eventual cross-linking between the two PI layers on the mechanical properties of the structures.

The height profiles over the patterned structure, as well as over the unpatterned control samples, were determined with a mechanical profilometer (Veeco Dektak 150, USA). The samples were mechanically released from the silicon carrier at the end of the fabrication process and tested with a 4000 Multipurpose Bondtester (Nordson DAGE, United Kingdom) using a 10 kg cartridge and pulled to fracture at a rate of 400 μm s^{-1}.

Tensile Bending: Test samples for the mechanical characterization of the CF/PI composite consist of a layer of carbonized PAN fibers on 6 μm thick PI (spin-coated at 3000 rpm, soft cured at 120 °C for 3 min, fully cured at 450 °C for 15 min) and cut with a scalpel into 5 mm × 10 mm pieces. The bend tester is a custom-made apparatus that consists of a fixated plate and a parallel one which moves in vertical direction at defined distance and frequency. The bending radius was chosen to be 3 mm (a radius found also in the somatosensory motor cortex of a rat).[56] The electrical resistance of the samples was measured with a hand multimeter (Agilent U1241B, USA) before bending, after 10, 50, and 100 k bending cycles.

Aging: PI/PI and CF/PI samples were subjected to accelerated aging in H_2O_2. They were stored in 30 mmol H_2O_2 (Karl Roth GmbH, Germany) + PBS solution (Sigma-Aldrich, USA) for one week at 37 °C in a dry chamber (Heraeus, Germany) to mimic the acute postsurgery inflammatory reaction in the first week after implantation.

Electrochemical Characterization of the ECoG Array: Flexible carbon ECoG devices were electrochemically characterized by connecting them to a ZIF connector (Hirose FH26W-17S-0.3SHW(60), Japan) mounted on a PCB. 180 μm thick PI tape (Kapton, RS Components GmbH, Germany) was placed on the connection pad area to ensure a tight fit of the thin-film devices into the ZIF connectors.

EIS was performed with a potentiostatic three-electrode setup in PBS solution (Sigma-Aldrich, USA). A silver/silver chloride electrode (Basi MF2052, USA) was used as reference electrode and a stainless-steel plate (2.3 × 2.3 cm^2, 0.5 mm thick) as counter electrode. The potentiostat (Metrohm Autolab, Switzerland) was given a sinusoidal input signal of 100 mV and the frequency was swept from 100 kHz to 1 Hz. CV was performed with the same setup used for the EIS. A determination of the electrodes water window was conducted by sweeping the input potential from −2 to +2 V at a scan rate of 20 mV s^{-1}. CV was instead done with a cathodic vertex potential of −0.9 V and an anodic vertex potential of +1.1 V at a scan rate of 50 mV s^{-1}.

In vitro biphasic pulse stimulation of the electrodes was performed with a PlexStim electrical stimulator system (Plexon, USA) in PBS. Charge-balanced biphasic cathodal first current pulses were pushed through the electrode against a platinum counterelectrode 20 million times. Pulse width was set to 200 μs, current to 30 μA, interpulse delay to 10 μs, and the repetition frequency to 200 Hz.

In Vivo Validation: The experimental plan was designed in compliance with the guidelines established by the European Communities Council (Directive 2010/63/EU, Italian Legislative Decree n. 26, 4/3/2014) and the protocol was approved by the Ethics Committee for animal research of the University of Ferrara and by the Italian Ministry of Health (authorization n 332/2015-PR).

Device functionality for neural applications was tested on one adult Long Evans rat (400–500 g) in three different positions over the S1BF. The surgical procedure to expose the rat barrel cortex (A-P: between 1 and 4 mm from bregma, M-L: between 3 and 5 mm from the midline), implant the array and record SEPs were performed using the protocols described elsewhere.[15] To calculate the SNR, the signal power was estimated by computing the integral of the spectral power density (SPD in the 3–1000 Hz band) of the signal (evoked activity, 60 intervals of 100 ms after the whiskers stimulation) and the noise power computed as the integral of the SPD of the noise (spontaneous activity, 60 intervals of 100 ms before the whiskers stimulation). Finally, the SNR was defined as the ratio between the signal power and the noise power.

Supporting Information

Supporting Information is available from the Wiley Online Library or from the author.

Acknowledgements

The authors sincerely thank Bettina Hunzinger, Institute of Advanced Materials, KIT for help with electrospinning, Erich Müller, Laboratory of Electron Microscopy, KIT for STEM analysis, and Thomas Lottner for his generous help with MR image acquisition. S.S. acknowledges financial support from the Ministry of Science, Research and Arts, Baden-Württemberg, Germany via Grant No. Az:33-7533-30-20/3/3, HEiKA Center FunTECH-3D. Part of the work was funded in the Cluster of Excellence BrainLinks-BrainTools (Deutsche Forschungsgemeinschaft-DFG, EXC 1086).

Conflict of Interest

The authors declare no conflict of interest.

Author Contributions

S.S. and T.S. contributed equally to this work. M.V. contributed to initial conception of the idea and fabrication process, electrochemical characterization of neural device, neural device manufacturing, and manuscript writing. C.G. contributed to neural device manufacturing, carbon fiber mat fabrication, electrochemical characterization of neural device, and mechanical device characterization. E.Z. and L.F. contributed to design and performance of animal experiments and performance of recordings. J.B.E. contributed to concept and performance of MR imaging. S.S. contributed to conception of idea, formulation of initial experiments, carbon fiber mat fabrication and characterization, and manuscript writing. T.S. contributed to scientific supervision of concept, experiments and manuscript, scientific advice in experiments, and editing of manuscript.

Keywords

bioelectronic medicine, carbon fibers, electrocorticography, micromachining, neural implants, polyimide

Received: August 20, 2019
Revised: November 12, 2019
Published online: December 11, 2019

[1] M. DiLuca, J. Olesen, *Neuron* **2014**, *82*, 1205.
[2] C. Bouton, *J. Intern. Med.* **2017**, *282*, 37.
[3] T. Stieglitz, *Neuroethics* **2019**, 1, https://doi.org/10.1007/s12152-019-09406-7.
[4] T. Stieglitz, in *Operative Neuromodulation* (Eds: D. E. Sakas, B. A. Simpson, E. S. Krames), Springer, Vienna **2006**, pp. 411–418.
[5] X. Navarro, T. B. Krueger, N. Lago, S. Micera, T. Stieglitz, P. Dario, *J. Peripher. Nerv. Syst.* **2005**, *10*, 229.
[6] W. M. Grill, S. E. Norman, R. V. Bellamkonda, *Annu. Rev. Biomed. Eng.* **2009**, *11*, 1.
[7] G. C. McConnell, H. D. Rees, A. I. Levey, C.-A. Gutekunst, R. E. Gross, R. V. Bellamkonda, *J. Neural Eng.* **2009**, *6*, 056003.

[8] N. J. Hill, T. N. Lal, M. Schroder, T. Hinterberger, B. Wilhelm, F. Nijboer, U. Mochty, G. Widman, C. Elger, B. Scholkopf, A. Kubler, N. Birbaumer, *IEEE Trans. Neural Syst. Rehabil. Eng.* **2006**, *14*, 183.
[9] C. A. Bosman, J.-M. Schoffelen, N. Brunet, R. Oostenveld, A. M. Bastos, T. Womelsdorf, B. Rubehn, T. Stieglitz, P. De Weerd, P. Fries, *Neuron* **2012**, *75*, 875.
[10] J. D. Yeager, D. J. Phillips, D. M. Rector, D. F. Bahr, *J. Neurosci. Methods* **2008**, *173*, 279.
[11] G. Buzsáki, C. A. Anastassiou, C. Koch, *Nat. Rev. Neurosci.* **2012**, *13*, 407.
[12] M. Vomero, M. F. P. Cruz, E. Zucchini, A. Shabanian, E. Delfino, S. Carli, L. Fadiga, D. Ricci, T. Stieglitz, *Conf. Proc. IEEE Eng. Med. Biol. Soc.*, July **2018**, *2018*, 4464.
[13] K. C. Cheung, *Biomed. Microdevices* **2007**, *9*, 923.
[14] S. F. Cogan, *Annu. Rev. Biomed. Eng.* **2008**, *10*, 275.
[15] M. Vomero, E. Zucchini, E. Delfino, C. Gueli, N. Mondragon, S. Carli, L. Fadiga, T. Stieglitz, *Materials* **2018**, *11*, 2486.
[16] S. Nimbalkar, E. Castagnola, A. Balasubramani, A. Scarpellini, S. Samejima, A. Khorasani, A. Boissenin, S. Thongpang, C. Moritz, S. Kassegne, *Sci. Rep.* **2018**, *8*, 6958.
[17] D. Ashouri Vajari, M. Vomero, J. Erhardt, A. Sadr, J. Ordonez, V. Coenen, T. Stieglitz, *Micromachines* **2018**, *9*, 510.
[18] W. Lee, V. Parpura, *Progress in Brain Research*, Elsevier, Amsterdam **2009**, pp. 110–125.
[19] L. Amato, L. Schulte, A. Heiskanen, S. S. Keller, S. Ndoni, J. Emnéus, *Electroanalysis* **2015**, *27*, 1544.
[20] E. Fuhrer, A. Bäcker, S. Kraft, F. J. Gruhl, M. Kirsch, N. MacKinnon, J. G. Korvink, S. Sharma, *Adv. Healthcare Mater.* **2018**, *7*, 1700915.
[21] K. Kinoshita, *Carbon: Electrochemical and Physicochemical Properties*, Wiley, New York **1988**.
[22] S. Sharma, *Materials* **2018**, *11*, 1857.
[23] T. D. Y. Kozai, N. B. Langhals, P. R. Patel, X. Deng, H. Zhang, K. L. Smith, J. Lahann, N. A. Kotov, D. R. Kipke, *Nat. Mater.* **2012**, *11*, 1065.
[24] E. Castagnola, N. Winchester Vahidi, S. Nimbalkar, S. Rudraraju, M. Thielk, E. Zucchini, C. Cea, S. Carli, T. Q. Gentner, D. Ricci, L. Fadiga, S. Kassegne, *MRS Adv.* **2018**, *3*, 1629.
[25] D. Kuzum, H. Takano, E. Shim, J. C. Reed, H. Juul, A. G. Richardson, J. de Vries, H. Bink, M. A. Dichter, T. H. Lucas, D. A. Coulter, E. Cubukcu, B. Litt, *Nat. Commun.* **2014**, *5*, 5259.
[26] M. Vomero, I. Dryg, T. Maxfield, W. Shain, S. Perlmutter, S. Kassegne, *ECS Trans.* **2016**, *72*, 91.
[27] G. Guitchounts, J. E. Markowitz, W. A. Liberti, T. J. Gardner, *J. Neural Eng.* **2013**, *10*, 046016.
[28] F. Torrisi, T. Hasan, W. Wu, Z. Sun, A. Lombardo, T. S. Kulmala, G.-W. Hsieh, S. Jung, F. Bonaccorso, P. J. Paul, D. Chu, A. C. Ferrari, *ACS Nano* **2012**, *6*, 2992.
[29] B. Fadeel, C. Bussy, S. Merino, E. Vázquez, E. Flahaut, F. Mouchet, L. Evariste, L. Gauthier, A. J. Koivisto, U. Vogel, C. Martín, L. G. Delogu, T. Buerki-Thurnherr, P. Wick, D. Beloin-Saint-Pierre, R. Hischier, M. Pelin, F. Candotto Carniel, M. Tretiach, F. Cesca, F. Benfenati, D. Scaini, L. Ballerini, K. Kostarelos, M. Prato, A. Bianco, *ACS Nano* **2018**, *12*, 10582.
[30] S. Sharma, C. N. Shyam Kumar, J. G. Korvink, C. Kübel, *Sci. Rep.* **2018**, *8*, 16282.
[31] D. B. Fischbach, *Carbon* **1967**, *5*, 565.
[32] M. Vomero, E. Castagnola, F. Ciarpella, E. Maggiolini, N. Goshi, E. Zucchini, S. Carli, L. Fadiga, S. Kassegne, D. Ricci, *Sci. Rep.* **2017**, *7*, 40332.
[33] M. Vomero, E. Castagnola, J. S. Ordonez, S. Carli, E. Zucchini, E. Maggiolini, C. Gueli, N. Goshi, F. Ciarpella, C. Cea, L. Fadiga, D. Ricci, S. Kassegne, T. Stieglitz, *Adv. Biosyst.* **2018**, *2*, 1700081.
[34] P. Wilhite, A. A. Vyas, J. Tan, J. Tan, T. Yamada, P. Wang, J. Park, C. Y. Yang, *Semicond. Sci. Technol.* **2014**, *29*, 054006.
[35] E. R. Mamleyev, S. Heissler, A. Nefedov, P. G. Weidler, N. Nordin, V. V. Kudryashov, K. Länge, N. MacKinnon, S. Sharma, *npj Flexible Electron.* **2019**, *3*, 2.
[36] M. Vomero, A. Oliveira, D. Ashouri, M. Eickenscheidt, T. Stieglitz, *Sci. Rep.* **2018**, *8*, 14749.
[37] X. Mao, T. Hatton, G. Rutledge, *Curr. Org. Chem.* **2013**, *17*, 1390.
[38] C. Kim, K. S. Yang, M. Kojima, K. Yoshida, Y. J. Kim, Y. A. Kim, M. Endo, *Adv. Funct. Mater.* **2006**, *16*, 2393.
[39] K. Naito, Y. Tanaka, J.-M. Yang, Y. Kagawa, *Carbon* **2008**, *46*, 189.
[40] S. Jain, T. J. Webster, A. Sharma, B. Basu, *Biomaterials* **2013**, *34*, 4891.
[41] J. Lee, S. Y. Lee, J. Jang, Y. H. Jeong, D.-W. Cho, *Langmuir* **2012**, *28*, 7267.
[42] N. Zander, *Polymers* **2013**, *5*, 19.
[43] P. Bajpai, *Carbon Fibre from Lignin*, Springer, Singapore **2017**.
[44] S. K. Martha, N. J. Dudney, J. O. Kiggans, J. Nanda, *J. Electrochem. Soc.* **2012**, *159*, A1652.
[45] P. Bhatt, A. Goe, *Mater. Sci. Res. India* **2017**, *14*, 52.
[46] F. Vitale, S. R. Summerson, B. Aazhang, C. Kemere, M. Pasquali, *ACS Nano* **2015**, *9*, 4465.
[47] C. S. Sharma, A. Sharma, M. Madou, *Langmuir* **2010**, *26*, 2218.
[48] X. Qian, X. Wang, J. Zhong, J. Zhi, F. Heng, Y. Zhang, S. Song, *J. Raman Spectrosc.* **2019**, *50*, 665.
[49] A. C. Ferrari, *MRS Proc.* **2001**, *675*, W11.5.1.
[50] D. Khodagholy, J. N. Gelinas, T. Thesen, W. Doyle, O. Devinsky, G. G. Malliaras, G. Buzsáki, *Nat. Neurosci.* **2015**, *18*, 310.
[51] J. A. Badwey, M. L. Karnovsky, *Annu. Rev. Biochem.* **1980**, *49*, 695.
[52] B. Halliwell, *J. Neurochem.* **1992**, *59*, 1609.
[53] M. G. Street, C. G. Welle, P. A. Takmakov, *Rev. Sci. Instrum.* **2018**, *89*, 094301.
[54] J. E. B. Randles, *Discuss. Faraday Soc.* **1947**, *1*, 11.
[55] M. Vomero, E. Castagnola, J. S. Ordonez, S. Carli, E. Zucchini, E. Maggiolini, C. Gueli, N. Goshi, L. Fadiga, D. Ricci, S. Kassegne, T. Stieglitz, in *2017 8th Int. IEEE EMBS Conf. on Neural Engineering (NER)*, IEEE, Shanghai, China **2017**, pp. 288–291.
[56] G. Paxinos, C. Watson, *The Rat Brain in Stereotaxic Coordinates*, Academic Press/Elsevier, Amsterdam/Boston **2007**.